LA-UR-16-22179

Title: Non destructive examination of UN / U-Si fuel pellets using neutrons
            (preliminary assessment)

Author(s): Bourke, Mark Andrew M.
            Vogel, Sven C.
            Voit, Stewart Lancaster
            Mcclellan, Kenneth James
            Losko, Adrian S.
            Tremsin, Anton

Intended for: Report

Issued: 2016-03-31

Non destructive examination of UN / U-Si fuel pellets using neutrons (preliminary assessment)

Fuel Cycle Research & Development

Prepared for U.S. Department of
Energy Campaign or Program

Sven C. Vogel, Adrian S. Losko,
Stewart L. Voit, Anton Tremsin,
Mark A.M. Bourke,
Kenneth J. McClellan.

Los Alamos National Laboratory

March 20, 2016

LA-UR-16-XXXX

SUMMARY

Tomographic imaging and diffraction measurements were performed on nine pellets; four UN/ U Si composite formulations (two enrichment levels), three pure U_3Si_5 reference formulations (two enrichment levels) and two reject pellets with visible flaws (to qualify the technique). The U-235 enrichments ranged from 0.2 to 8.8 wt.%. The nitride/silicide composites are candidate compositions for use as Accident Tolerant Fuel (ATF). The monophase U_3Si_5 material was included as a reference. Pellets from the same fabrication batches will be inserted in the Advanced Test Reactor at Idaho during 2016.

The goal of the Advanced Non-destructive Fuel Examination work package is the development and application of non-destructive neutron imaging and scattering techniques to ceramic and metallic nuclear fuels. Data reported in this report were collected in the LANSCE run cycle that started in September 2015 and ended in March 2016. Data analysis is ongoing thus this report provides a preliminary review of the measurements and provides an overview of the characterized samples.

Key preliminary results include:

- Neutron resonance analysis (using Tantalum for normalization) determined isotopic enrichment levels to within 0.1 at% of fabrication values
- Five of seven production pellets were homogeneous to the spatial resolution of the measurements
- One composite pellet shows an inclusion or incipient crack
- One composite pellet shows a density variation of a few % with a maximum on the center plane of the pellet
- 3D characterization of cracks, flaws and isotopic distributions are determined non destructively in complete pellets to spatial resolutions of at least 100 microns
- 3D characterization of cracks, flaws and density distributions in complete ATF pellets are possible in 3 to 4 hours.
- 3D characterization of isotopic distributions are possible in complete ATF pellets in 3 to 5 days.
- Measurements of crystallographic phase, texture and spatially resolved measurements were completed but have not been analyzed.

CONTENTS

FIGURES

TABLES

ACRONYMS

AECL	Atomic Energy of Canada Limited
APS	Advanced Photon Source
AFC	Advanced Fuel Cycle
ATF	Accident Tolerant Fuel
ATR	Advanced Test Reactor
BWR	Boiling Water Reactor
CCD	Charge-Coupled Device
CEA	French Alternative Energies and Atomic Energy Commission
DOE	Department of Energy
DOT	Department of Transportation
EBS	Ethylene bis-stearate
EPMA	Electron Probe Microanalysis
FCCI	Fuel Cladding Chemical Interaction
FCMI	Fuel Cladding Mechanical Interaction
FCRD	Fuel Cycle Research and Development
FOV	Field of View
FR	Fast Reactor
HEU	Highly Enriched Uranium
HFEF	Hot Fuels Examination Facility
HI	High Intensity
HIPPO	High Pressure/Preferred Orientation neutron diffractometer
IAEA	International Atomic Energy Agency
IMCL	Irradiated Materials Characterization Laboratory
INL	Idaho National Laboratory
JAEA	Japan Atomic Energy Agency
LANL	Los Alamos National Laboratory
LANSCE	Los Alamos Neutron Science Center
LEU	Low enriched uranium
LWR	Light Water Reactor
MA	Minor Actinides
MAMOX	Minor Actinide bearing Mixed Oxide Fuels
MOX	Mixed Oxide Fuels
NDE	Non-Destructive Evaluation

ND-PIE	Non-Destructive Post Irradiation Examination
NPDF	Neutron Powder Diffractometer/Neutron Pair Distribution Function
NRC	Nuclear Regulatory Commission
NRC	National Research Council Canada
NSLS	National Synchrotron Light Source
ORNL	Oak Ridge National Laboratory
O/M	Oxygen-to-Metal ratio
PCMI	Pellet Cladding Mechanical Interaction
PIE	Post Irradiation Examination
pRAD	Proton Radiography
PSI	Paul Scherrer Institute
PWR	Pressurized Water Reactor
RE	Rare Earth element
ROI	Region of Interest
SEM	Scanning Electron Microscopy
SMARTS	Spectrometer for Materials Research at Temperature and Stress
TFRE	Transmutation Fuel with Rare earth inclusions
TMRS	Target-Moderator-Reflector System
TEM	Transmission Electron Microscopy
TOF	Time-of-flight
UN	Uranium nitride
U-Si	Uranium silicide (unspecified stoichiometry)
US	United States

1.   Introduction

1.1   Science-based Approach to Nuclear Fuel Development

A key enabler for a "science based approach" for accelerated development and certification of new, accident tolerant nuclear fuels is an early and efficient understanding of material behavior at multiple length scales. For new fuel formulations, there is a dearth of irradiation testing experience. When representative irradiation tests take years it is important to extract the maximum insight possible from each test. Post irradiation examination (PIE) of fuels is mature and sophisticated but measurements in hot cells are expensive and typically examine small volumes of irradiated fuels. This leaves the possibility that key failure inducing phenomena will not be observed because of limited PIE. For these reasons there is value in techniques that can quickly and non-destructively characterize properties over volumes consistent with standard fuel geometries. Such techniques can inform models on the initial condition of samples and complement, guide, and leverage destructive post irradiation examination. For example three dimensional characterization of complete fuel pellets within cladding after irradiation could identify regions that are representative of average and atypical response.

Typical in-pile irradiation tests of new fuel types last months or years. Demands on PIE may also impose a delay of years before individual samples can be studied. The resulting levels of radioactivity even for rodlets containing just a handful of pellets require hot cells and remote manipulators to perform destructive PIE. The complexity and cost of such operations limit the PIE possible thus there is a premium on knowing where to measure. This research is focused on developing techniques to non destructively examine rodlets containing multiple pellets.

The first step in the project is to "benchmark" the initial condition of candidate materials before irradiation. The second step will be to make comparable measurements on irradiated rodlets prior to their destructive examination in INL hot cells. Neutron, proton and (synchrotron) X-ray radiography / tomography techniques all pose opportunities for this endeavor. By virtue of their stand-off capability and ability to probe materials despite an intense gamma field neutrons and protons both offer potential for study of highly radioactive materials. At Los Alamos neutron based techniques are routinely used to evaluate microstructure, phase and composition and protons are widely used for dynamic radiography.

The programmatic emphases for developing advanced non-destructive evaluation (ANDE) techniques applicable to irradiated materials are two-fold. First it will be possible to evaluate fuel rods to guide the destructive post-irradiation examination towards regions of interest that are not obvious with conventional techniques. This will help develop the statistical insight necessary to complement modeling and simulation data. Adding ANDE insight to the standard optical, thermal neutron and gamma ray insights will help identify regions where destructive examination can be focused. This will increase the return from PIE since regions of atypical irradiation performance are more likely to be discovered. A second reason for ANDE lies in the desire to generate data as soon as possible after removal of the test samples from the reactor. This is a key requirement in accelerating the development and time to licensing of new fuel forms. The philosophy is consistent with improving diagnostics to offer faster turnaround and getting "more out of less". Programmatically, the capabilities under development sets the stage for routine pre-irradiation fuel evaluation and potentially for post-irradiation evaluations of Accident Tolerant Fuels (ATF).

The techniques employed at LANSCE use the pulsed neutron source at the Lujan center may. They rely on collocation with the 800MeV proton accelerator. However advances in laser based neutron sources with small-scale accelerators for neutron generation (by D-D fusion) or laser-drive pulsed neutron

sources[1] pose interesting opportunities. Although such small scale sources are not currently capable of neutron production for measurements of the type described here technological advance is ongoing. It is possible that, in the next decade, a "small-scale" accelerator source with sufficient neutron production performance might become available to provide "pool side" implementation of the techniques described in this report.

1.2   **Scope and Goals of this activity**

One method to enhance accident tolerance of the fuels is to improve the thermal conductivity to reduce the fuel centerline temperature. This increases the time to reach critical temperature in an accident. At LANL a composite of UN with 15-vol% U_3Si_5 is under consideration as a potential ATF forms[2][3]. In the current work accident tolerant fuels systems based on composites of U_3Si_5 and UN were fabricated, encapsulated in a cladding/capsule configuration and examined with a variety of neutron based techniques to establish their ability to accurately measure chemistry, phase content and isotope distribution, as well as defects and flaws within the ATF pellets. The rodlet geometry matches the configuration that will be used for testing these fuels in the Advanced Test Reactor.

Pre-existing inclusions, density, chemical and isotopic inhomogeneities and cracks as well as microstructural features such as phase composition, texture or residual stresses can affect fuel behavior in an irradiation environment. For science based development initiatives it is hoped that certification of new fuel systems can be achieved by fusing science insight with insights from fewer irradiation tests than has been true in the past. However the goal of accelerated insight from fewer tests places more emphasis on pre-characterizing the condition of test fuel samples prior to irradiation as well as the need for more thorough bulk characterization of the whole irradiated volume to guide destructive examination of irradiated materials. Since neutrons are non destructive, capable of interrogating whole pellets and sensitive to the mesoscale characteristics being implemented in models, they are uniquely suited for the study of prototype nuclear fuels. Non destructive 3D maps of cracks, density, isotopic and geometry variation can be measured using neutrons in pellets prior irradiation. The potential exists for making the same measurements post irradiation. The ultimate goal is to accelerate the time to insight, development and certification of new nuclear fuels.

This initiative is focused on the application of neutrons to draw non-destructive insight on fresh nuclear fuel prior to irradiation and in the future on irradiated fuel. Neutron imaging and scattering techniques easily examine volumes of up to several cubic centimeters, consistent with typical rod assemblies of ceramic fuel pellets. Neutron scattering lengths for high and low atomic number elements are often comparable and allow efficient study of systems consisting of heavy and light elements.

The application of protons and synchrotron X-rays are also under consideration for these studies (though not reported here). Protons like neutrons, have mean free paths in nuclear materials that facilitate characterization of cubic centimeters of material. The interaction of protons with matter is governed by nuclear and Coulomb interactions. They lose energy in the matter because of Coulomb scattering from the atomic electrons, and scatter from the nuclei both because of the strong interaction and the Coulomb interaction with the proton. Proton radiography is performed by illuminating a target object with a beam of protons and focusing the transmitted protons onto a scintillator screen[4]. Magnetic lenses offer different magnification options. Synchrotron X-rays in excess of 50KeV also have applicability to fresh nuclear fuels and have been used in the study of U-Mo fuel. This established their merit for studies of smaller regions of interest than are typically examined in neutron measurements. In future a holistic suite of measurement tools might naturally use neutrons, protons and synchrotron x-rays.

At a pulsed neutron sources time of flight energy sorting allows examination of samples by setting the contrast on isotopes or crystal structures. Neutron detector technology has been revolutionized by the use of micro-channel plates (MCPs) for radiographic applications and proved a catalyst for these studies. The micro-channels are coated with neutron absorbing materials such as boron. They currently offer a spatial resolution of 55μm at count rates of 10^8 cm^{-2}s^{-1}. Spatial resolution of 15μm has been demonstrated at lower count rates [5].

At a LANL/INL workshop held in December of 2012 a plan was conceived to use the advanced non-destructive evaluation techniques including neutron and proton radiography available at LANL and INL for analysis of irradiated fuel rodlets from the AFC-2C irradiation at the ATR in Idaho[6]. In the first phase a set of mock-up rodlets were examined containing pellets of depleted uranium dioxide (dUO$_2$) with defects similar to that seen in irradiated fuel rodlets. After these first measurements over the last few years, measurements have demonstrated the applicability of neutrons, protons and synchrotron X-rays to a range of ceramic and metallic fuels. Several terabytes of imaging and scattering data have been collected. The ability to observe cladding dimensions, cracks, phase and isotopic species nondestructively and in three dimensions has been demonstrated. Development in data analysis and instrumentation is ongoing.

Tomographic analysis of typical fuel clad geometries using only thermal neutrons can elucidate three dimensional heterogeneities in a few hours. Whereas determination of isotopic species requires measurements of resonances in the epithermal range and measurements on typical clad/pellet geometries typically require a few days of beam time for between 3 and 6 pellets. Diffraction characterization in slices through the sample provides valuable additional information at beam times of about 0.5 days. Although early work focused on UO$_2$ recent initiatives have focused on developing fuels with enhanced accident tolerance, increased burn-up and reduced waste.

2.   Neutron Analysis

2.1   Neutrons

Neutrons offer excellent characterization capabilities for nuclear fuels and provide non-destructive insight on mechanical integrity, microstructure, chemistry and crystallographic phase. Measurements are possible at reactors or pulsed sources, but the energy resolution is implicit at pulsed sources and offers capability not efficiently pursued at reactor sources. Recent advances in 2D neutron detection enable improved opportunities for imaging and tomography of nuclear materials. Moreover, time-of-flight (TOF) neutron measurements enable isotope specific tomography. Isotopic densities are deduced from transmission spectra exhibiting neutron resonances, which are recorded for each pixel. Tomographic algorithms allow 3D reconstructions of the spatial distribution of isotopes as well as density and feature heterogeneities. The ability to perform radiographs at 1eV and above improves capability for samples that are less effectively examined with thermal neutrons. By using epithermal neutron energies and assuming known total neutron cross sections of constituents, isotopic enrichment levels can be determined.

Neutrons interact with the nucleus rather than the atomic shell, thus, their interaction characteristics differ markedly from X-rays. Fig. 1 illustrates this by showing penetration depths as a measure of interaction potential for all elements with neutrons, X-rays, and electrons. The data explain why neutron measurements are more sensitive to light elements in the presence of uranium than X-ray measurements. Since the scattering lengths of neutrons for high and low Z-number elements are comparable in many cases they are more effective in resolving the elemental contribution of for example uranium and silicon. By contrast in X-rays diffraction the scattered intensity is biased towards the heavier element. Indeed, for structural analyses of Urania determined by diffraction techniques reported and collected in the Inorganic Crystal Structure Database, of the 66 experimental structure records for Urania, UO$_{2+x}$, 55% were

measured using neutron diffraction. Neutrons measurements routinely characterize samples as small as a few mm^3 or as large as cm^3.
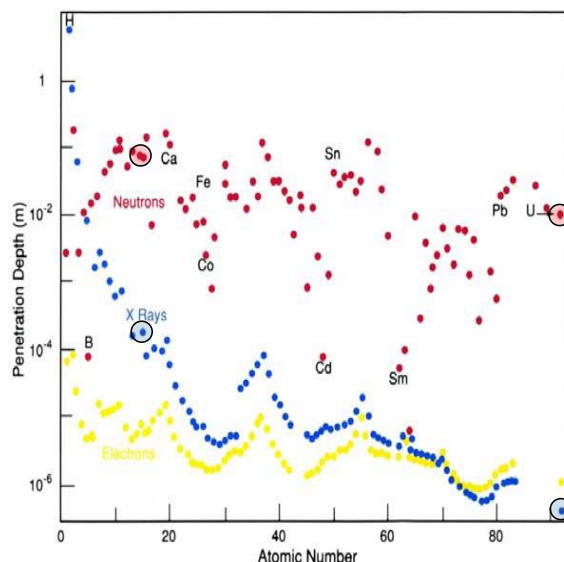
Fig. 1: **Penetration depth vs element atomic number; neutrons (red), X-rays (blue), and electrons (yellow). Circles highlight Silicon (number 14) and Uranium (number 92).**

2.2 **Neutron radiography**

Imaging with neutrons, protons and X-rays has been applied at LANL to demonstration nuclear fuels since 2010 [7] [8] . The primary focus remains on neutrons because of their isotopic sensitivity, their applicability to cm^3 size samples and their potential application to irradiated material. At a pulsed neutron source neutron absorption resonances act as finger-print of isotopes. Energy-resolved neutron imaging, enabled by time-of-flight (TOF) neutrons, can be used in various energy ranges. For example, Lehmann et al. described energy-selective neutron imaging using thermal and cold neutrons for quantification [9]. "Energy-dependent neutron imaging with a double crystal monochromator at the ANTARES facility at FRM II" is described by Schulz et al with neutron wavelengths ranging from 2.7 to 6.5°A [10]. Strobl et al. describe advances in energy-selective imaging in detail in their review "Advances in neutron radiography and tomography" [11]. With sufficient penetration and resolution, tomographic methods provide nondestructive measures of voids, cracks, density variations. Reconstruction of features requires the ability to compute a three-dimensional picture from attenuation-based density variations of a series of two-dimensional radiographs.

2.3 **Tomographic reconstruction**

2.3.1 **Data Processing**

The detector employed for the energy-resolved neutron imaging and tomography stores several thousand frames corresponding to defined neutron time-of-flight or energy values. Subsequent handling and manipulating the data for tomographic reconstruction is challenging. A significant challenge in developing the routine application of this capability lies in provision of facile user access to the breadth of

interpretive opportunity. A few examples are listed below each of which requires considerable data manipulation.

- Integration over a thermal energy window offers maximum spatial resolution in minimum time (due to spectral characteristics of the Lujan source)
- Integration over a broad epithermal energy range may offer good spatial resolution if resonances from one or more isotopes dominates.
- Integration across one or more discrete energy windows may offer isotopic sensitivity.
- Spectral fitting can be applied to pixel average data or single detector pixels

After raw radiographs are produced for any of the options above, tomographic reconstructions are possible provided multiple projections were collected. The tool used for the 3D- reconstruction in these measurements was TomoJ which is a plugin for the image analysis tool ImageJ. It is a free software package that was originally designed for electron tomography. In our experience it compared well with commercial reconstruction tools, such as Octopus or VGStudio.   To prepare transmission vs. energy spectra for fitting the raw data was background corrected and divided by open-beam. Scaling factors (determined from an open beam measurement) were included for individual detector pixels.

Tomographic projections are prone to ring artifacts and when they were observed a ring-filter was applied. This process first required a polar transform of the reconstructed images (normal to the cylinder axis of the pellets and the rotation axis for the tomography scan). Then a one-dimensional median filter was applied with a length of 30pixels along the stripes. The polar-transformed image was divided by the resultant median-filtered-polar-transformed image to remove the ring artifacts. Finally the images were transformed back into Cartesian coordinates and the filtered slices were normalized to the original grey-values. An example of the ring-filter is shown in Fig. 2.
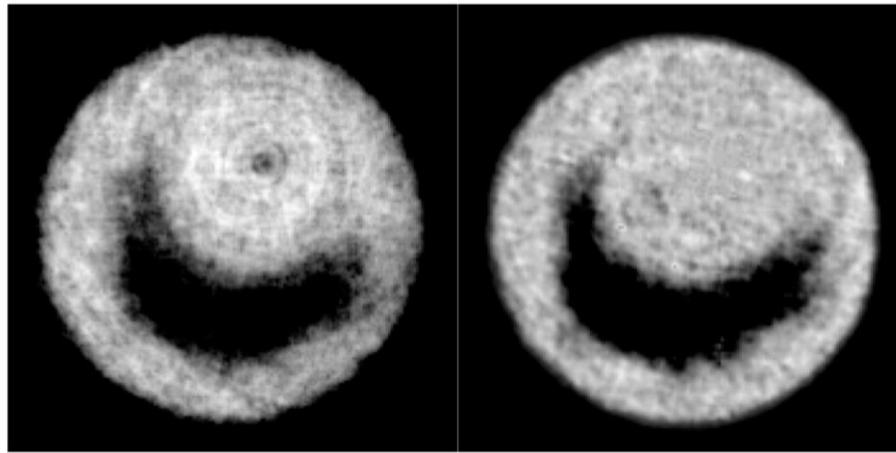
Fig. 2:   The effect of the "Ring filter" is shown above on a single slice for pellet 4; Before (left) and after (Right).

The ring filter improves the quality of the CT reconstruction and the use of an internal standard provides the ability to quantify the density of isotopes, including determination of the enrichment level. For reasons described below Tantalum proved best suited for this purpose. It has several narrow resonances in the 1 to 200eV energy range and a foil of known thickness was measured simultaneous with the rodlets. By including a known aerial density for the Tantalum the SAMMY resonance fit (described below) can accurately fit the energy dependent background.

2.3.2 Thermal and Epithermal neutron spectrum

The neutron beam on flight path 5 at the Lujan provides thermal and epithermal neutrons with each pulse. The moderator is optimized for the thermal spectrum (<0.4 eV). In this region, individual projections can take as little as one minute to acquire sufficient counting statistics. Measurements of neutron resonances are typically performed at >1eV for which count-times per projection typically require between 30 and 180 minutes for good enough statistics to allow the fits shown in Fig. 17 thru Fig. 21.

Thus thermal imaging is an effective and "quick" way to identify the presence of cracks, whereas epithermal imaging of resonances requires longer acquisition times but provides isotope specific insight. Since data for both energy regions are collected simultaneously, the long count times for resonance imaging also provide high quality thermal radiographs. The energy resolution ΔE/E of a measurement dictates the ability to resolve individual neutron absorption resonances. This results in a tradeoff between source to sample distance and energy resolution.

2.3.3 Resonance Cross sections from ENDF

Energy dependent neutron cross sections due to nuclear resonances provide the material signature necessary for isotope imaging. An enabling capability for these measurements are the tabulated nuclear cross sections in the Evaluated Nuclear Data File (ENDF) database [12]. This provides cross sections, determined by standardized experimental measurements such as neutron transmission measurements, for individual isotopes. In general, neutron resonances are measurable in a regime of 1ev to 0.1 MeV. Below 1eV cross sections are typically inversely proportional to the velocity of the neutron and do not exhibit "sharp" resonances. For energies greater than 0.1MeV resonances cannot be resolved experimentally.

2.3.4 Resonance fitting by SAMMY

Resonance spectra recorded in this study were fit using the SAMMY code (SAMMY, Multilevel R-Matrix Fits to Neutron and Charged-Particle Cross Section Data)[13]. This code was developed by Oak Ridge National Laboratory. It can analyze time-of-flight, cross section data from meV to MeV, where the incident particle is either a neutron or a charged particle. For energies up to several KeV, cross sections are generated using the Reich-Moore approximation to R-matrix theory [14]. The code includes a variety mechanisms to account for normalization, background, and sample thickness as well as options to account for measurement resolution and Doppler broadening. Corrections for self-shielding and multiple-scattering are also available.

Resolved resonance parameters can be outputted in the ENDF format for inclusion in the evaluated nuclear data files. Bayes' Theorem of generalized least squares is used to find "best fit" values of parameters and the associated parameter covariance matrix. After data are normalized they are fit with SAMMY. The data input consists of an ENDF database input file with pre-determined resonance parameters (literature values of energies, capture and partial widths and spin numbers as well as the sample element's name, atomic weight and energy range for the data set). Background parameters (constant, linear in energy and time) are varied to account for the efficiency and response of each individual pixel.

When the sample thickness is large compared with respect to the cross section of the resonance for a given energy, the sample can absorb all incident neutrons in a discrete energy range. This causes the transmission to drop to zero and the resonances are described as "black". For attenuation based imaging, a fully absorbed beam will appear as an opaque feature in the transmission image, making tomographic reconstruction impossible since the depth information is lost. However, for resonance imaging, reconstruction with black resonances remains possible by considering energy regions around the

resonance. Indeed in that case black resonances help identify the background for transmission in the epithermal range.

2.4   Calculating enrichment levels from resonance data

To interpret transmission data correctly, it is essential that the "background" is treated accurately for proper data normalization. As a consequence, normalization of the spectrum is essential if absolute values of areal densities are desired. If the background is not accounted for artificial intensity is assumed in each projection and results in an error for absolute areal density. For this work a scaled open-beam profile was used as a "baseline" background. The normalized data were then treated with the SAMMY code [15]. The resonance parameters provided by the ENDF database were treated as constants. Background parameters (constant, linear in energy and linear in time) were varied to account for the efficiency and response of individual detector pixels. Then the areal density of different constituents were varied, from which absolute isotopic densities were determined.

2.5   Neutron diffraction

Imaging is complemented by diffraction, which provides insight on crystal structure (space group, lattice parameters, atomic positions, thermal motion etc.), phase volume fractions, lattice strains (mechanical strain, chemical strain from e.g. interstitial atoms, etc.) and texture (orientation distribution of crystals). For neutron powder diffraction data analysis, typically full pattern "Rietveld" refinements are performed. From these crystal structure (lattice parameters, atomic positions etc.), microstructure (sample induced peak broadening, phase fractions, texture etc.), and instrument (background, instrument contributions to peak broadening etc.) can be determined.

3.   Instrumentation

3.1   Flight Path 5 (for imaging)

Imaging measurements described in this report were performed using Flight-Path-5 (FP5) at the Lujan Neutron Scattering Center (for a description see M. Mocko et al [16]). It provides a thermal neutron flux of ~ 2.4 10^7n·cm^{-2}s^{-1} at ~8.8m from the moderator with a peak at 25meV. The beam is collimated using borated polyethylene and steel disks with a circular exit collimator. For the measurements reported here the detector was positioned ~ 8.2 m from the source. The fuel rodlets were placed as close as possible to the detector to maximize the collimation ratio, L/D. A collimator to sample distance L of about 2m and beam diameter of 2cm gave a collimation ratio of approximately 100.   Samples are mounted on a rotation stage with a linear motion stage, allowing translation of the sample in multiple directions (Fig. 4).
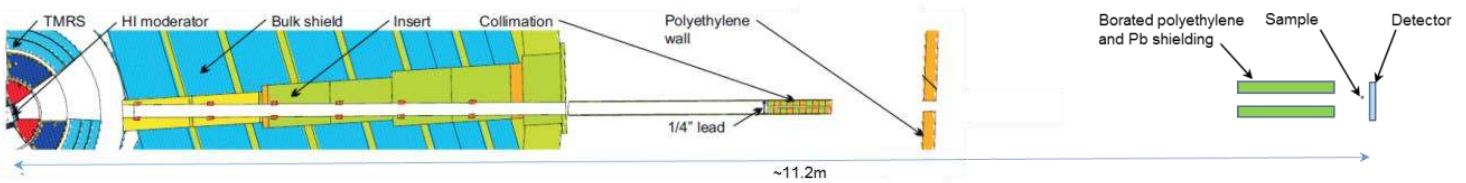
Fig. 3:   Flight Path 5 Schematic
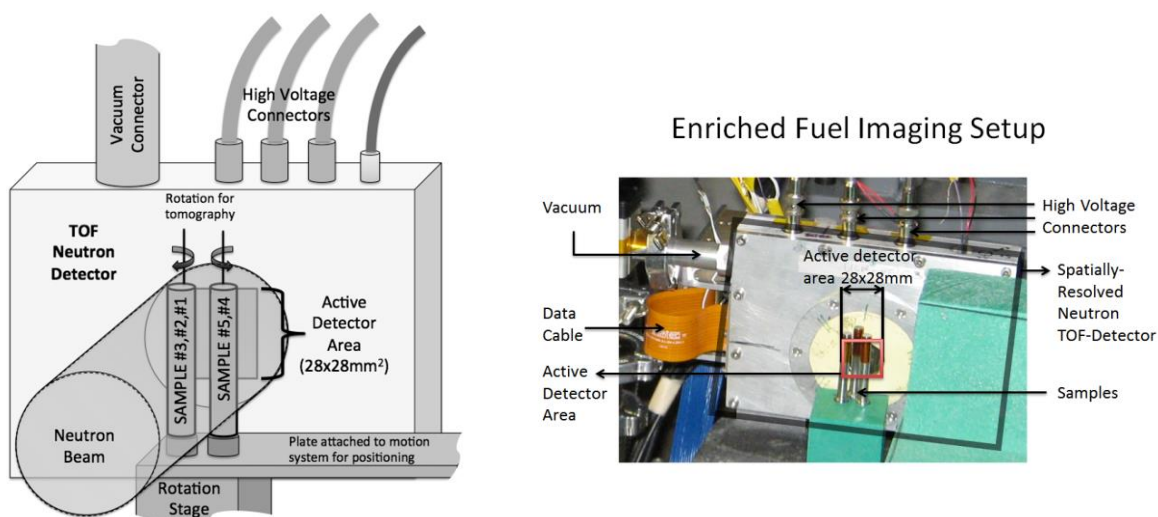
Fig. 4:   Rodlets in front of detector; Schematic (left), Photograph (Right).

The pixilated neutron time-of-flight imaging detector used at LANL is custom-designed and manufactured by Dr. A. Tremsin (Space Science Laboratory, UC Berkeley). It consists of a Gd/B doped multi-channel plate and MediPix read-out chip [17]. To account for differences in the individual pixel response of the detector, an open-beam measurement was recorded over the entire energy range (0.5 to 200eV). Individual TOF images are divided by the normalized open-beam image. The pixel size of the detector is 55μm with an active area of 512x512 pixels i.e. ~ 28 x28 mm^2.

3.2   **HIPPO (for diffraction)**

Two instruments were used for diffraction studies on the ATF fuels; HIPPO and SMARTS (for spatially resolved measurements). The HIPPO instrument is a general purpose neutron time-of-flight powder diffractometer. Its key characteristics are large detector coverage (1200 ^{3}He detector tubes distributed on 53 panels arranged on five rings around the incident beam) and proximity to the neutron source (~8.9 meters). The short flight path and detector coverage and allow count times as short as one minute and efficient texture characterization. The resolution (Δd/d) in the back scattering geometry is ~ 0.0037 and the 20Hz repetition rate of the Lujan Center source accesses a d-spacing range from 0.12 to 22°A.   A robotic arm is available for sample changes.
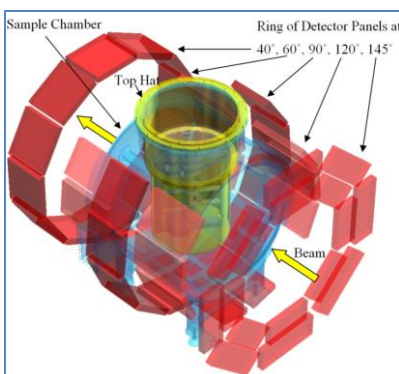
Fig. 5:   HIPPO ; Schematic of general purpose neutron powder diffractometer.

4.   FY15 measurements on ATF and Transmutation fuels

4.1   Crystal Structure, Composition and Texture in UN / U-Si

In FY15 studies of crystal structure were performed on samples of ATF fuels fabricated with depleted Uranium. Rietveld refinement provided spatially resolved characterization of various crystallographic and microstructural parameters. The results indicated variations in chemistry between pellets. Texture evaluation indicated no preferred orientation in the UN phase, but showed a strong preferred orientation in the U_3Si_5.

A UN 15vol% U_3Si_5 pellet was scanned in 2mm steps along the length of the rodlet with 2mm vertical spatial resolution slit. A typical data set is shown in Fig. 6. Data (red), Rietveld fit (green) and difference curve (magenta) are displayed. The data were collected with the HIPPO 144° detector panels, data collected in the other detectors was analyzed simultaneously (i.e. the structural parameters are a fit to data from several detectors) but is not shown here. The phases for the Rietveld fit were γ-Fe (stainless steel), cubic UN, and hexagonal U_3Si_5.   Refined parameters included; weight fractions of the three phases, lattice parameters/unit cell volume of the three phases, peak width of the steel and UN/U_3Si_5, thermal motion parameters of the Fe, U, and Si/N atoms (the latter were constrained to a single thermal motion parameter for numerical stability of the analysis).
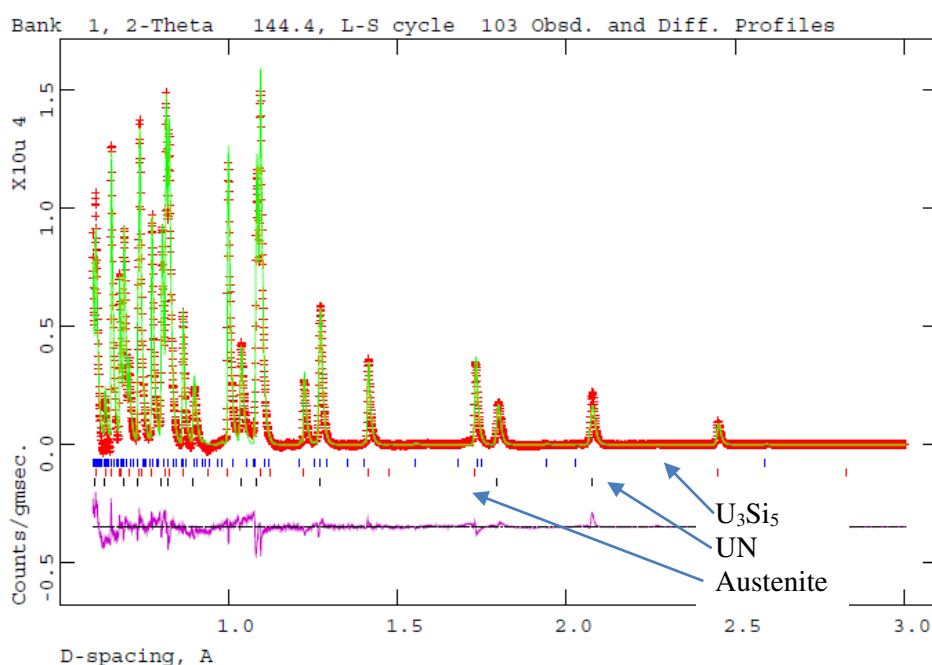
Fig. 6:   Diffraction from a 2mm slice of the ATF. Ticks mark calculated peak positions for austenite (black), UN (red), and U_3Si_5 (blue).

A series of 2mm high scans were executed across 5 pellets. Fig. 7 shows the variation of the UN lattice parameter as a function of sample height (the first two data points were only partially illuminated, resulting in larger scatter). For the third to seventh data point a significant difference in lattice parameter is noted. This is consistent with a difference in chemistry of the bottom pellet compared to the remaining pellets.
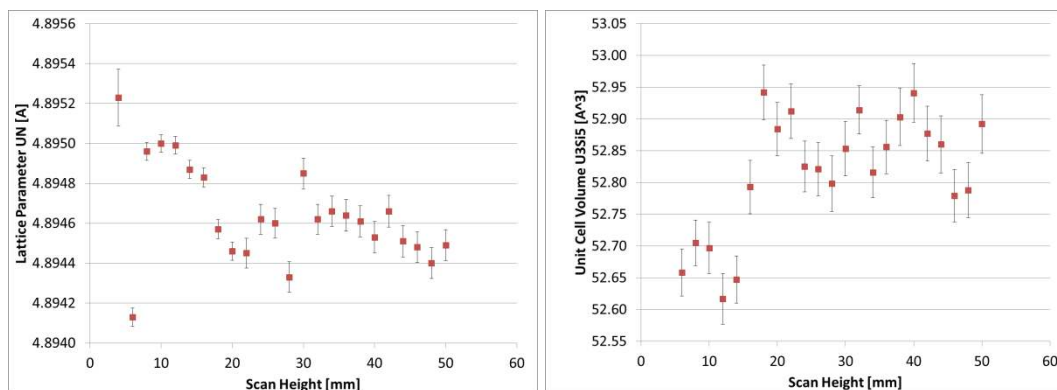
Fig. 7:   UN lattice parameter as function of height (left) and U₃Si₅ unit cell volume (2mm scan height over 5 ATF pellets).

Texture measurements through the same slices indicated that the UN phase, for these samples, exhibited a preferred orientation that is close to random whereas the U_3Si_5 phase exhibited either substantial preferred orientation – or large grains (i.e. the probed volume consists of few U_3Si_5 grains). Fig. 8 shows the pole figures from a full texture refinement of a single slice. Each U_3Si_5 grain has one c-axis (002) and three a-axis poles (200). The U_3Si_5 pole figures therefore indicate that the probed volume consists of ~3 grains as there are three maxima present in the 002 pole figure. The UN pole figures confirm the absence of preferred orientation qualitatively derived from the raw diffraction data. The cylinder axis of the pellets and the rodlet is perpendicular to the paper.

UN   U₃Si₅
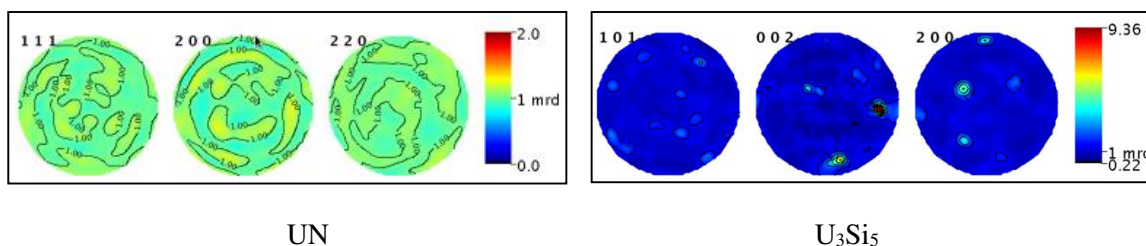
Fig. 8:   Pole figures, UN (left) and U₃Si₅ (right).

4.2   **Rare earth inclusions in transmutation fuel**

U-10Zr slugs were fabricated at INL with three levels of rare earth (RE) additions; 0, 1, and 5 at%. The composition of the RE lanthanide mix was reported in the previous milestone report. The RE mix was added to the U-10Zr and cast into a slug. At INL, the U-10Zr samples were placed inside HT-9 rodlets and sealed with sodium (to aid in thermal transport). The rodlets were then welded inside a secondary capsule. Fig. 9 shows the welded rodlets. These rodlets were made for demonstration purposes and approximated irradiation geometries, but were not fabricated to meet engineering tolerances necessary for ATR insertion.

Neutron tomography identified regions of rare earth inclusions. Tomographic features noted in thermal radiography were relate to the increase or absence of ^{238}U and Nd in resonance tomographs. Discrete rare earth inclusions are resolved with resonance reconstructions. An example of a tomographic reconstruction is included in Fig. 10. The metallic slug is double encapsulated in 316L stainless steel capsule and HT-9 rodlet. The image shows the thermal neutron reconstruction (left), Nd resonance energy reconstruction (center, slug dimensions indicated by dashed red line), and the ^{238}U resonance energy reconstruction (right).

Fig. 9: U-10Zr- 5% RE slug (left) and Rodlets containing metallic fuel slugs (right).

Thermal	^{145} Nd Resonance	^{238}U Resonance*
$\int_0^{\sim 50 meV}$	$\int_{4.29\,eV}^{4.31\,eV}$	$\int_{6.0\,eV}^{6.5\,eV} + \int_{7.25\,eV}^{6.75\,eV}$
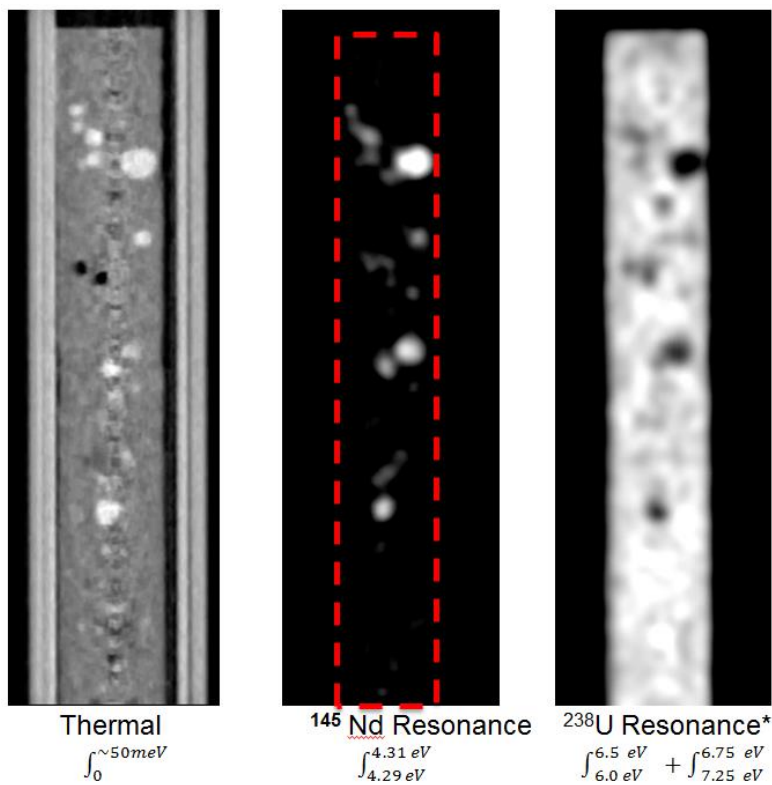
Fig. 10: Thermal and epithermal imaging of U-10Zr transmutation fuel with 5% rare earth (lanthanide mix) inclusion.

5.   Pellet fabrication and Rodlet assembly

5.1   Synthesis

U$_3$Si$_5$ and UN-15v%U$_3$Si$_5$ fuel pellets were prepared using conventional powder metallurgical methods as outlined in the flow diagrams shown in Fig. 11. The feedstock for the U$_3$Si$_5$ pellets was prepared by arc-melting stoichiometric amounts of uranium (8.84% enriched in U-235) and silicon metals followed by a heat treatment to homogenize the phase content. The silicide was then crushed, ground, and the powder sieved to -44μm.
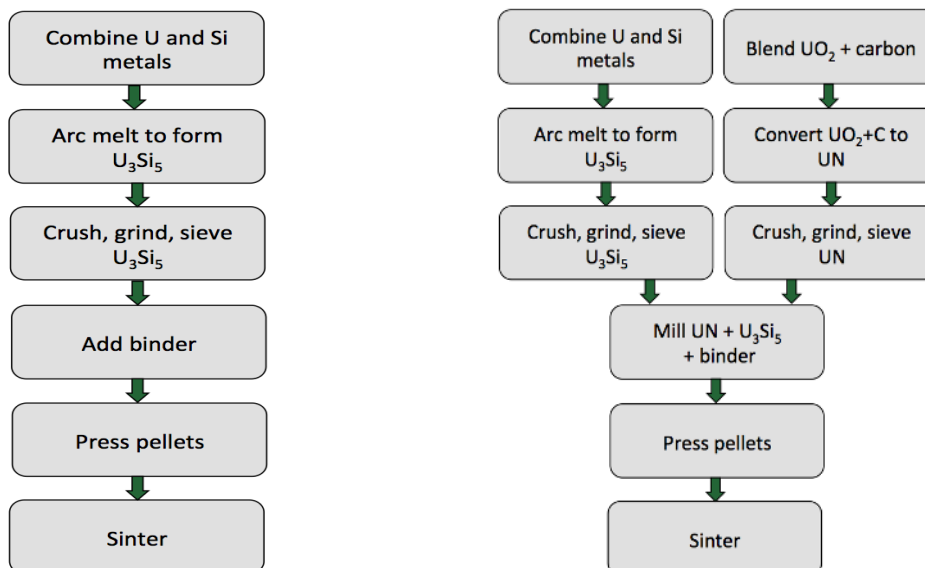
Fig. 11: Pellet fabrication flow diagrams; U$_3$Si$_5$ (Left), UN-15v%U$_3$Si$_5$ (Right))

The powder binder EBS (ethylene bis stearamide) was blended with the sieved U$_3$Si$_5$ powder. Individual powder charges were loaded into a die then pressed at 100 MPa into simple right cylinders. Green pellets were then sintered for 12 hours at 1515°C under flowing argon to a theoretical density of >90%. The UN-15v%U$_3$Si$_5$ pellets were fabricated by first synthesizing the UN and U$_3$Si$_5$ feedstock materials then subsequently milling the feedstock powders, pressing the powder into pellets at 100MPa, and sintering for 12 hours at 1775°C under flowing argon to achieve high density pellets.

Two different uranium enrichment schemes were used in the fabrication of UN-15v%U$_3$Si$_5$ pellets. In one batch of pellets, the U-235 enrichment of the UN was fixed at a nominal LWR (Light Water Reactor) fuel value of 4.9%. The enrichment of the corresponding U$_3$Si$_5$ phase was 8.84% to give an overall uniform U-235 density across the fuel. In the second batch of UN-15v%U$_3$Si$_5$ pellets, the U-235 enrichment was set to 2.7% in both the UN and U$_3$Si$_5$ and given the difference in material densities the UN phase has a higher U-235 density than the U$_3$Si$_5$ phase.

5.2   **Pellets**

During the 2015/2016 LANSCE run cycle measurements were performed on nine pellets. Four UN/ U$_3$Si$_5$ pellets (3 of one enrichment level and one of a second). Two UN/ U$_3$Si$_2$ pellets (of a single enrichment level), three monolithic U$_3$Si$_5$ pellets (with two enrichment levels). The UN/U-Si composite compositions reflect candidate accident tolerant fuel compositions. The U$_3$Si$_5$ is studied as a reference to complement the studies on the composites. Pellets for study were selected in varying conditions with and without end cap defects to help understand the capability.

The composition, phase fraction and 235-U enrichments for the nine pellets are listed in Table 1below. The four UN U$_3$Si$_5$ pellets weighed approximately 6.5g. The two UN U$_3$Si$_2$ pellets weighed approximately 5.6 g. The three U$_3$Si$_5$ pellets weighed between 4 and 4.6g. All pellets were approximately 9mm in length and 8mm in diameter.

Composition	Pellet ID	U Enrichment (wt. %)			Rodlet #	Position in rodlet	Batch ID (Voit)	Lujan - Pellet ID
		UN	U$_3$Si$_5$	U$_3$Si$_2$				
UN (15 Vol% U$_3$Si$_5$)	1	2.70	2.70	N/A	1	(1 of 3, Cap up -Top)	Lujan LANL-1-27-27	UN-U3Si5 (2.7,2.7) Rod 1, Pel 1/3 t
	9				3	(1 of 2, Cap down -Top)	COMP1-Lujan3	UN-U3Si5 (2.7,2.7) Rod 3 Pel 1/2 t
	8				3	(2 of 2, Cap down Bottom)	COMP1-Lujan3	UN-U3Si5 (2.7,2.7) Rod 3 Pel 2/2 b
UN (15 Vol% U$_3$Si$_5$)	7	4.95	8.84	N/A	4	(1 of 2, Cap down-Top)	COMP2-Lujan4	UN-U3Si5 (4.95,8.84) Rod 4 Pel 1/2 t
UN (30 *Wt* % U$_3$Si$_2$)	4	4.1	N/A	4.9	2	(1 of 2, Cap up Top)	Lujan WEC-1	UN-U3Si2 (4.1,4.9) Rod 2 Pel 1/2 t (WEC)
	5				2	(2 of 2, Cap up Bottom)	Lujan WEC-2	UN-U3Si2 (4.1,4.9) Rod 2 Pel 2/2 b (WEC)
U$_3$Si$_5$ (100 Vol %)	2	N/A	8.84	N/A	1	(2 of 3, Cap up Middle)	Lujan LEU3SI5	U3Si5-LEU (8.8) Rod 1 Pel 2/3 m
	6				4	(2 of 2, Cap down Bottom)	LEU3SI5-Lujan4	U3Si5-LEU (8.8) Rod 4 Pel 2/2 b
U$_3$Si$_5$ (100 Vol %)	3	N/A	0.20	N/A	1	(3 of 3, Cap up Bottom)	Lujan DU3SI5	U3Si5-DU (0.2) Rod 1 Pel 3/3 b

Table 1: As fabricated enrichment levels ; ATF pellets

5.3   **Rodlet / Pellet Assembly**

The pellets listed in Table 1 were assembled in four rodlets as described in Table 2 and shown schematically in Fig. 12.   The rodlets for these examinations were made of aluminum though previous measurements demonstrated capability on representative cladding. Aluminum spacers were inserted between the pellets to facilitate visualization. A spring and aluminum spacers were also included to reduce the potential for pellet rotation. The designation "cap up" and "cap down" in the table describes (an arbitrary) change in can orientation for the measurements. (For rodlets 1& 2 the cap was "up" and for rodlets 3&4 the cap was "down").

| Rodlet #	Position in rodlet	Pellet ID (Losko)	Composition	U Enrichment (wt. %)			Batch ID (Voit)	Lujan - Pellet ID
				UN	U3Si5	U3Si2		
1	(1 of 3, Cap up -Top)	1	UN - 15 Vol% U3Si5	2.70	2.70	N/A	Lujan LANL-1-27-27	UN-U3Si5 (2.7,2.7) Rod 1, Pel 1/3 t
	(2 of 3, Cap up Middle)	2	100 % U3Si5 (LEU)	N/A	8.84	N/A	Lujan LEU3SI5	U3Si5-LEU (8.8) Rod 1 Pel 2/3 m
	(3 of 3, Cap up Bottom)	3	100 % U3Si5 (DU)	N/A	0.20	N/A	Lujan DU3SI5	U3Si5-DU (0.2) Rod 1 Pel 3/3 b
2	(1 of 2, Cap up Top)	4	UN 30 Wt % U3Si2	4.1	N/A	4.9	Lujan WEC-1	UN-U3Si2 (4.1,4.9) Rod 2 Pel 1/2 t (WEC)
	(2 of 2, Cap up Bottom)	5	UN 30 Wt % U3Si2	4.1	N/A	4.9	Lujan WEC-2	UN-U3Si2 (4.1,4.9) Rod 2 Pel 2/2 b (WEC)
3	(1 of 2, Cap down -Top)	9	UN 15 Vol% U3Si5	2.70	2.70	N/A	COMP1-Lujan3	UN-U3Si5 (2.7,2.7) Rod 3 Pel 1/2 t
	(2 of 2, Cap down Bottom)	8	UN 15 Vol% U3Si5	2.70	2.70	N/A	COMP1-Lujan3	UN-U3Si5 (2.7,2.7) Rod 3 Pel 2/2 b
4	(1 of 2, Cap down-Top)	7	UN 15 Vol% U3Si5	4.95	8.84	N/A	COMP2-Lujan4	UN-U3Si5 (4.95,8.84) Rod 4 Pel 1/2 t
	(2 of 2, Cap down Bottom)	6	100 % U3Si5 (LEU)	N/A	8.84	N/A	LEU3SI5-Lujan4	U3Si5-LEU (8.8) Rod 4 Pel 2/2 b

Table 2: Rodlet/pellet Assembly position
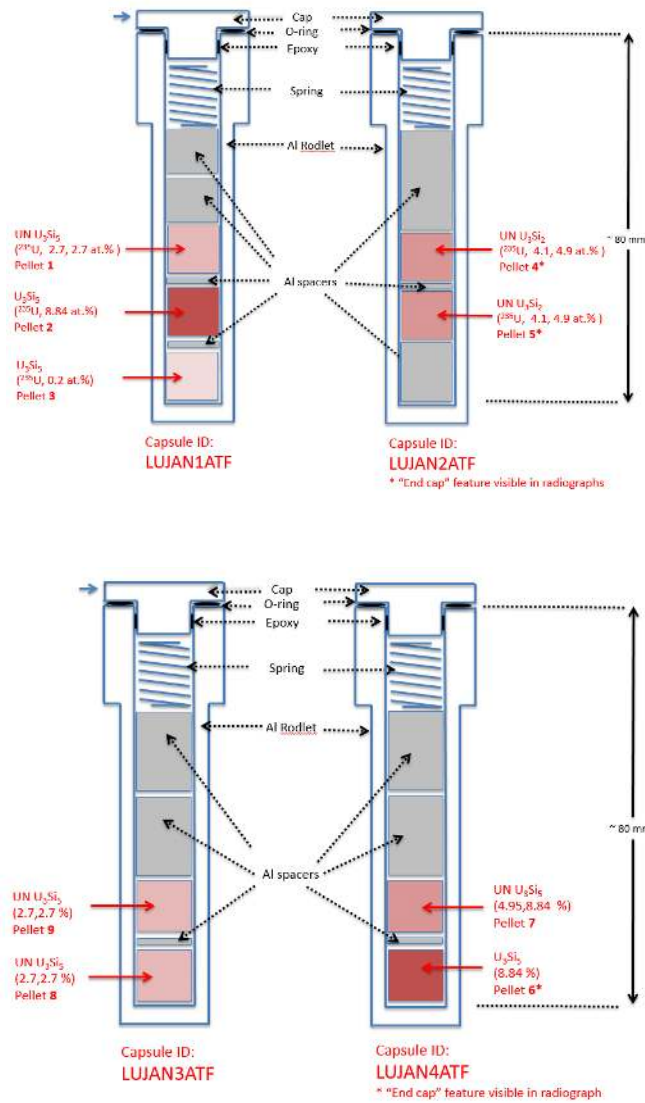
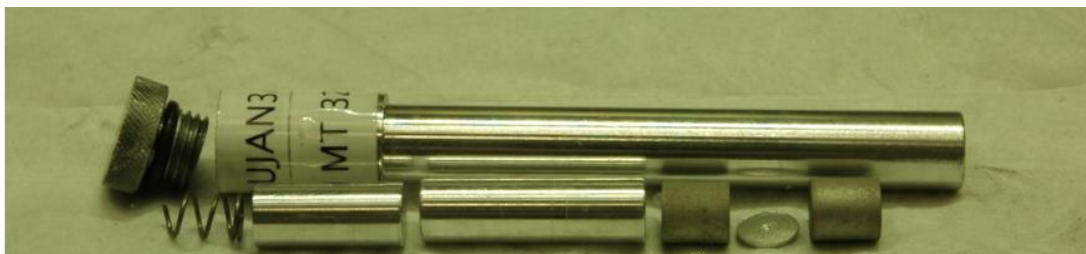Fig. 12: Rodlet/Pellet assembly schematics

Fig. 13: Rodlet 3 loading assembly configuration. From left to right; threaded cap, spring, two aluminum spacers, pellet, aluminum spacer and pellet.

6.   UN/ U-Si Preliminary results

6.1   Experiment Summary

Between October 2015 and March 2016 tomographic data collections were collected on rodlets 1 thru 4 listed in section 5 (Table 3). Data acquisition of 5 minute per projection were sufficient for tomographic reconstructions using thermal neutrons and for simultaneous reconstruction in the epithermal region data acquisition greater than 20 minutes was required. Diffraction measurements were performed on HIPPO and spatially resolved diffraction using SMARTS and will be reported in a future report.

Utilizing the time resolved neutron-beam at the Lujan Neutron Scattering Center, tomographic data-sets were recorded for the rodlets described in section 5. Typical data-sets consisted of 51 projections with an angular step-size of 3.6 degree per projection and 20 minutes integration time per projection. Transmission images were acquired in TOF-mode with a time-bin-width used to record the time of flight neutron data was set to 320ns. For measurement in the epithermal region data were recorded from 40 to 800µs in equal spaced time bins corresponding to an energy-range approximately from 207 to 0.6 eV.

	Rods	Date	Detector to source [m]	L/D	Acquisition/ Projections [min]	Cd-Filter	Total# Projections	Angular Step [degree]
FP-5	1&2	10/21/2015	11.20	260	20	Yes	100	1.8
FP-5	1&2	10/23/2015	8.26	113	45	Yes	50	3.6
FP-5	1&2	12/03/2015	8.50	125	20	Yes	200	0.9
FP-5	3&4		11.20	260	60	Yes	50	3.6
FP-5	3&4		11.20	260	5	No	100	1.8
FP-5	1&2		11.20	260	5	No	100	1.8

Table 3: Summary of neutron tomographic data collected during the 2015/2016 LANSCE run cycle

6.2   Measurements of isotopic enrichment.

Both 235-U and 238-U have resonances in the1 to 200 eV range that is easily accessible on FP5. In Fig. 14 the three strong resonances are for 238-U while many 235-U resonances are also apparent with cross sections up to 1000 barns. With calibration and SAMMY fitting an absolute determination is possible of the isotopic composition of any isotopes with resolved resonances. U-235 enrichment levels were determined for all pellets.

To calculate absolute measurements a calibrant is required. In the first test with rodlets 1 and 2 cadmium was tries as a calibrant because of its propensity to shield thermal neutrons and thus reduce the activation of the enriched fuel. However as is discussed below for Rodlets 3 and 4 Tantalum was used instead. Fig. 15 shows why Tantalum is a better choice due to the prevalence of Tantalum resonances in

the 1 to 50eV regime compared with a single Cd resonance in the same region (though it has more above 50eV).

For each pellet a region in the center of each pellet (see Fig. 16) was integrated from which an average enrichment value was determined. In Fig. 17 thru Fig. 21 the SAMMY fits for the region between 1eV and 50eV are shown for each pellet. SAMMY calculated enrichment levels are shown in Table 4. For Rodlets 3 and 4 Tantalum was used for normalization and the neutron measurement of the average enrichment was within 0.1 at % of the nominal fabrication values. For rodlets 1 and 2 which used Cadmium for normalization the neutron calculated ^{235}U enrichment levels showed a systematic underestimate of the enrichment levels. It is currently assumed that this disparity resulted from the weak presence of Cadmium resonances in the key region of 1 to 50eV. Ta works better because it has multiple strong and sharp resonances in the 1 to 50eV energy range providing a better determination of background. The nominal and measured ^{238}U areal density showed agreement within uncertainties.
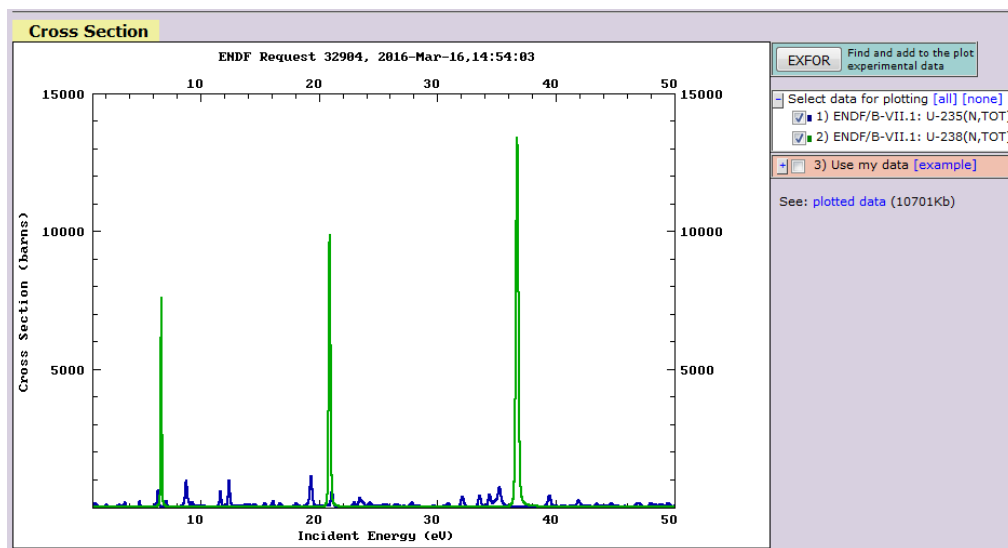
Fig. 14: U-235, U-238 resonances (ENDF 1 to 50eV)
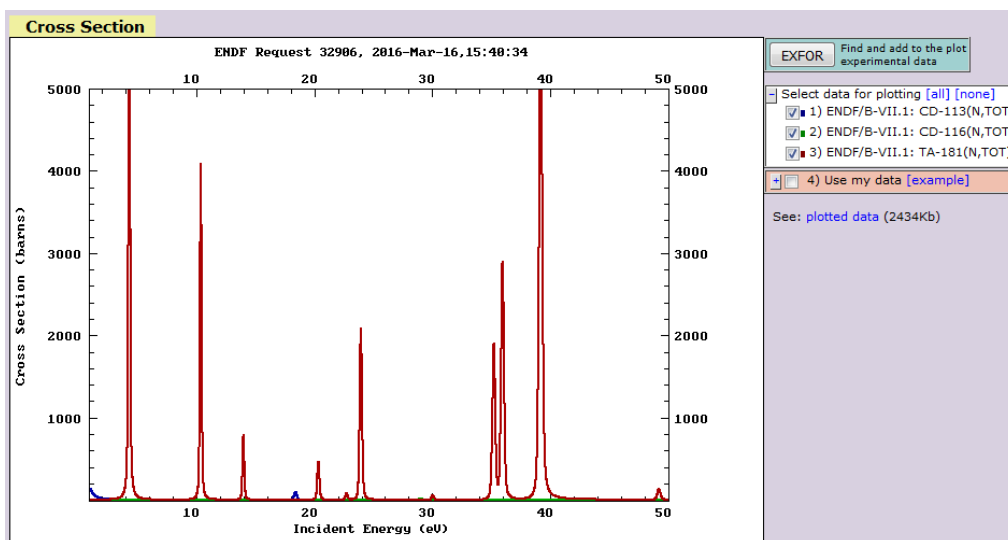
Fig. 15: Cd-113, Cd 116, Ta-181 resonances (ENDF 1 to 50eV)

Fig. 16: Attenuation image rodlets 1 and 2 (integrated from 0.5 to200 eV). The black rectangles indicate region used for SAMMY fits.

Fig. 17: UN 15 vol.% U₃Si₅ (2.7, 2.7% enrichment)   Pellet 1 (left) , Pellet 9 (center) , Pellet 8 (right). [Pellet 1 Cd normalization, Pellets 8 and 9 Ta normalization.]

Fig. 18: UN 15 vol% U₃Si₅ (4.95, 8.84 % enrichment) Pellet 7 (Ta normalization)

Fig. 19: UN 30 wt% U₃Si₂ (4.1, 4.9 % enrichment)   Pellets 4 (left) Pellet 5 (right) (Cd normalization)
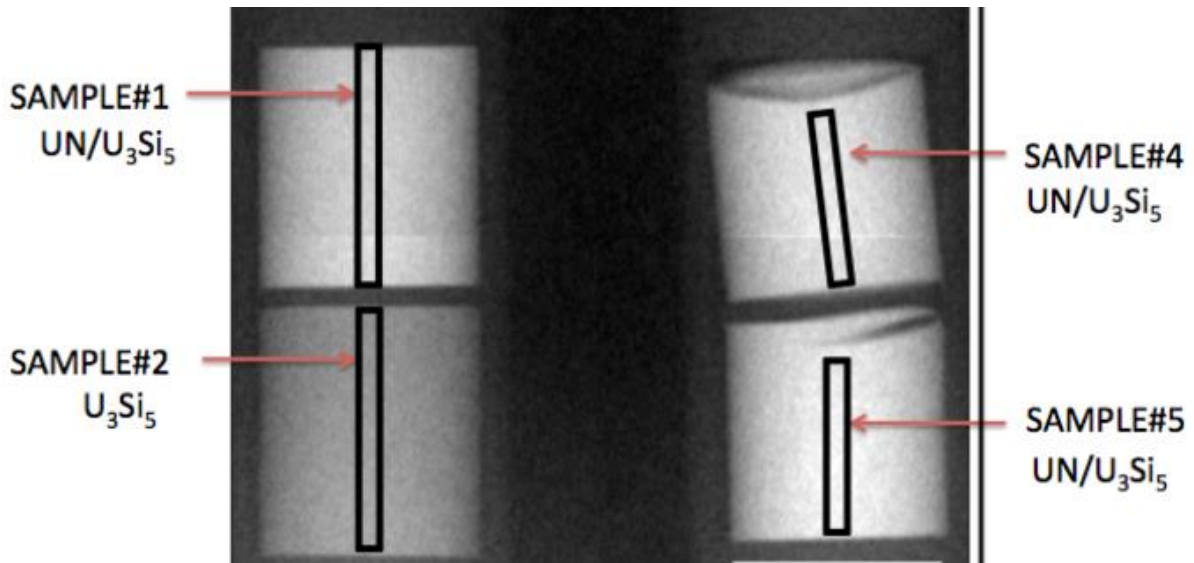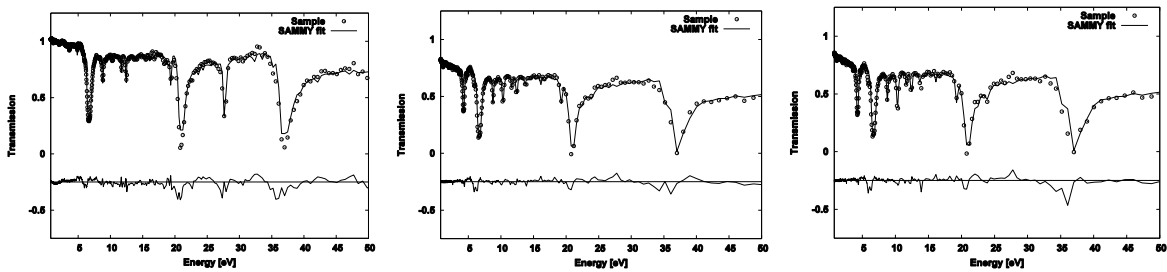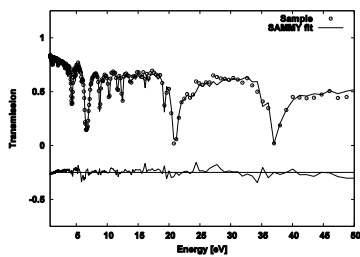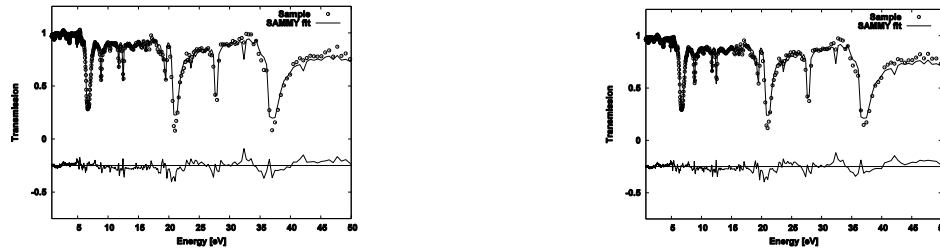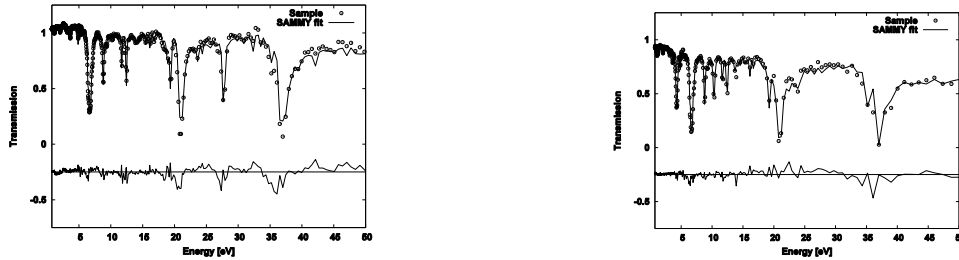

Fig. 20: U₃Si₅ (8.84 % enrichment)   Pellets 2 (left) 6 (right) [Pellet 2 Cd normalization, Pellet 6 Ta normalization]
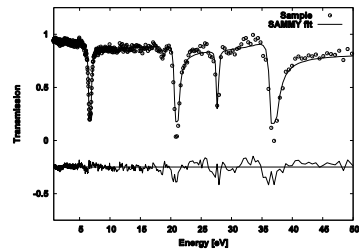
Fig. 21: U₃Si₅ (0.2 % enrichment)   Pellet 3 (Cd normalization)

Pellet #	Rod #	Normalization	Composition	235-U enrichment (wt %)		Comment
				Fabrication target	SAMMY measurement	
2	1	Cd	U₃Si₅ (100 Vol %)	8.84%	6.97%	Poor Background fit
4	2	Cd	UN U₃Si₂ (30 Wt%)	4.34%	3.72%	Poor Background fit
5	2	Cd	UN U₃Si₂ (30 Wt%)	4.34%	3.79%	Poor Background fit
1	1	Cd	UN U₃Si₅ (15 Vol%)	2.70%	2.27%	Poor Background fit
3	1	Cd	U₃Si₅ (100 Vol %)	0.20%	0.14%	Poor Background fit
6	4	Ta	U₃Si₅ (100 Vol %)	8.84%	8.68%	Good Background fit
7	4	Ta	UN U₃Si₅ (15 Vol%)	5.53%	5.58%	Good Background fit
8	3	Ta	UN U₃Si₅ (15 Vol%)	2.70%	2.65%	Good Background fit
9	3	Ta	UN U₃Si₅ (15 Vol%)	2.70%	2.65%	Good Background fit

Table 4: 235-U enrichment. As fabricated and Neutron resonance determination (SAMMY).

## 6.3	**Features observed in tomographic reconstructions**

The limiting spatial resolution of the tomographic characterization in the current measurement suite is dictated by the 55 micron pixel size in the detector. (The potential for improving this spatial resolution is discussed in section 7). Here preliminary observations of the current data set are presented focusing on the anomalies. A more comprehensive analysis will be discussed in the next milestone report.

Attenuation image of all nine pellets: Fig. 22 shows an attenuation image of all nine pellets (pellet 3 is truncated). A summary of the density heterogeneities is provided in Table 5. The overall homogeneity of density and pellet uniformity was within the current limiting spatial resolution of 55 microns of the technique with two exceptions (not including the reject pellets).

Oblate inclusion Pellet 9 (UN-U_3Si_5) show an oblate inclusion up to 100 microns in dimension that is visible in both thermal and epithermal tomographic reconstructions (Fig. 23). The rotation of the pellet was not maintained between the thermal and epithermal data which were collected in different runs and thus the feature appears at different locations in the figure. Fig. 24 includes a profile plot through the inclusion. The dimension of the inclusion in the vertical orientation is close to the spatial resolution of the technique and thus the dip in intensity observed in Fig 24 is consistent with a crack. Examination of this feature in the isotopic reconstructions should provide corroborating evidence on the nature of this heterogeneity.

Density Variation? Pellet 1 (UN-U_3Si_5) suggest a long range density variation that is a maximum on the center plane of the pellet and diminishes to either end. The effect is small but appears to exceed experimental error and is under examination (Fig. 25).

End cap cracks in reject pellets. Pellets 4 and 5 (UN-U_3Si_2) were both reject pellets. They were rejected because of visible end caps that extended across >50% of the pellet cross section. Sections through tomographic reconstructions are included in Fig. 26. Pellet 4 shows an incipient crack at one end that only weakly penetrated the surface and would likely have been hard to identify visually if it had been less well developed.

Contrast variation. One advantage of tomographic reconstructions is the ability to alter the contrast of the reconstructions to highlight different aspects of the reconstruction. This allows images that focus on features of interest though also means that the data needs to be interpreted by a skilled operator familiar with the materials science features of interest. In Fig. 27 two contrast settings are selected for rodlet 4.

Composition	Pellet ID	Crack	Comment	U Enrichment (wt. %)		
				UN	U_3Si_5	U_3Si_2
UN (15 Vol% U_3Si_5)	1	Homogeneous to < 100 microns	Possible density variation?	2.70	2.70	N/A
	9	Oblate inclusion ~ 100 microns	Incipient crack?			
	8	Homogeneous to < 100 microns				
UN (15 Vol% U_3Si_5)	7	Homogeneous to < 100 microns		4.95	8.84	N/A
UN (30 *Wt* % U_3Si_2)	4	End cap 50% penetration End cap 20% penetration	Reject pellet	4.1	N/A	4.9
	5	End cap 90% penetration	Reject pellet			
U_3Si_5 (100 Vol %)	2	Homogeneous to < 100 microns	Reference pellet	N/A	8.84	N/A
	6	Homogeneous to < 100 microns Divot off one end	Reference pellet			
U_3Si_5 (100 Vol %)	3	Divot off one end	Reference pellet	N/A	0.20	N/A

Table 5: Summary of preliminary observations from tomographic characterization

Rodlet 1
Pellet 1 UN U_3Si_5 (Top)
Pellet 2 U_3Si_5 (Middle)
Pellet 3 U_3Si_5 (Bottom)

Rodlet 2
Pellet 4 UN U_3Si_2 (Top)
Pellet 5 UN U_3Si_2 (Bottom)

Rodlet 3
Pellet 9 UN U_3Si_5 (Top)
Pellet 8 UN U_3Si_5 (Bottom)

Rodlet 4
Pellet 7 UN U_3Si_5 (Top)
Pellet 6 U_3Si_5 (Bottom)
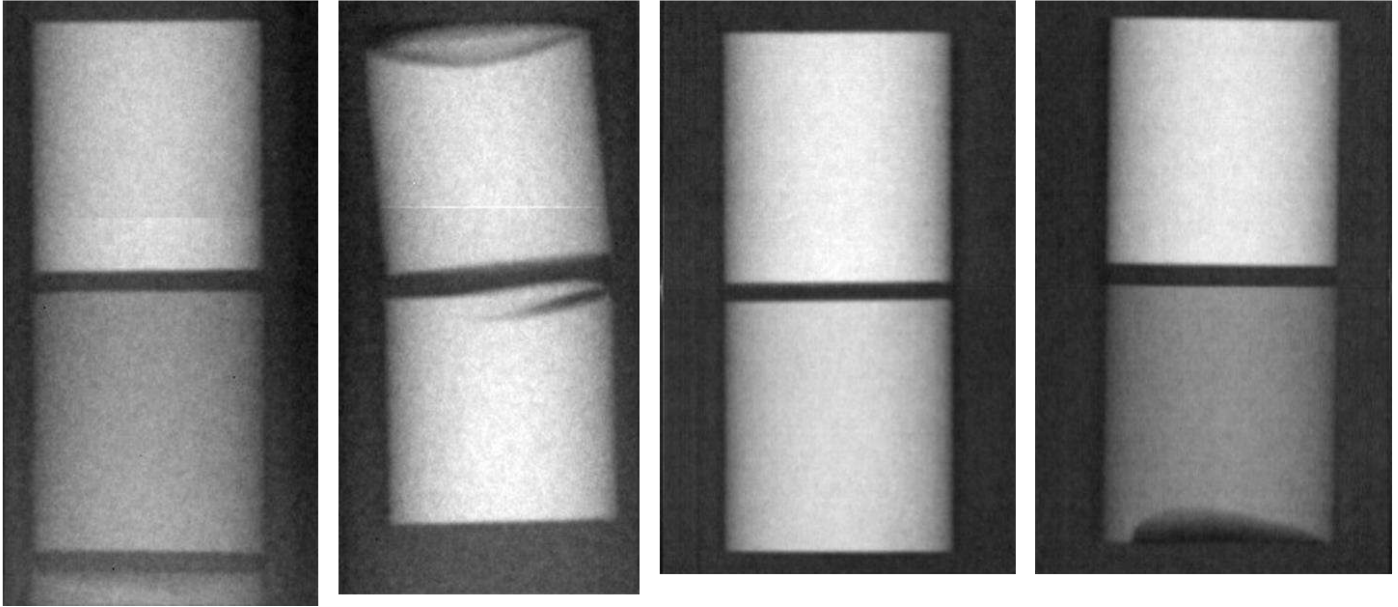
Fig. 22: Radiographic images of four rodlets (The cap is oriented at the top of the page for all images).

Epithermal
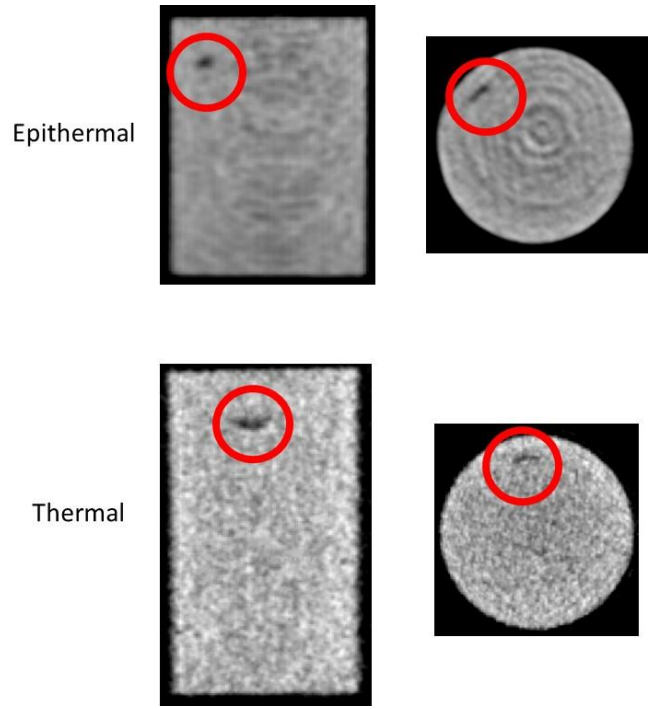
Thermal

Fig. 23: Pellet 9; Slices through side and plan view reconstructions showing a feature that is present in both the epithermal (top) and thermal reconstructions (bottom).
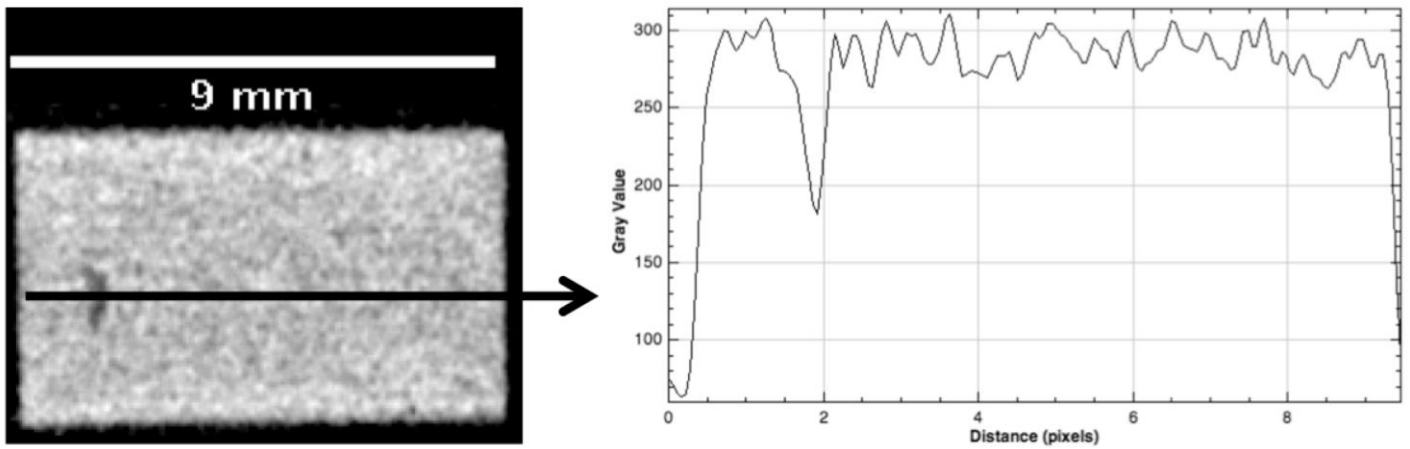
Fig. 24: Pellet 9. Profile plot of reconstructed slice through the feature shown in Figure 23..
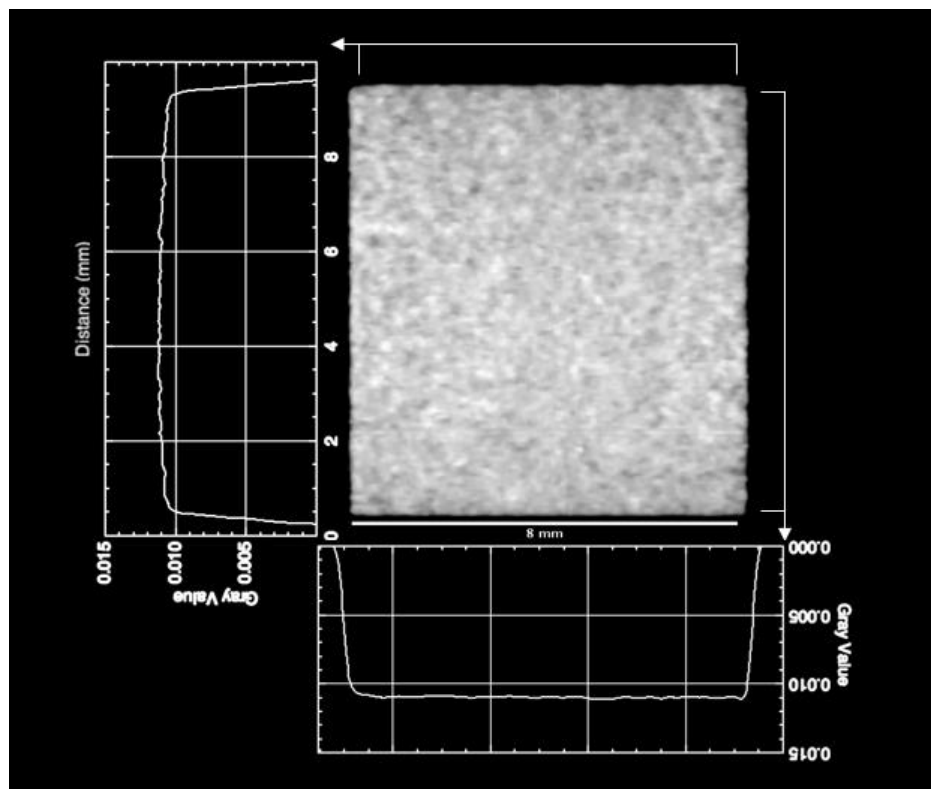
Fig. 25: Pellet 1 Sections through thermal reconstruction. The profile on the left of the pellet is consistent with a density variation that is maximum on the center horizontal plane of the pellet and diminishes to top and bottom.

Fig. 26: (Reject) Pellets 4 (top) and 5 (bottom) (Left). Pellet 4 lower region (Right)

Fig. 27: Rodlet 4 Contrast set to highlight divot in pellet 6 (left). Rodlet 4 contrast set to highlight Aluminum can (right)

7.   Discussion

Between October 2015 and March 2016, tomographic and diffraction data were recorded for nine ATF pellets. The pellets were removed from batches fabricated for irradiation and exemplified materials that both passed and failed quality control assessment for irradiation testing. Tomographic reconstruction is complex and in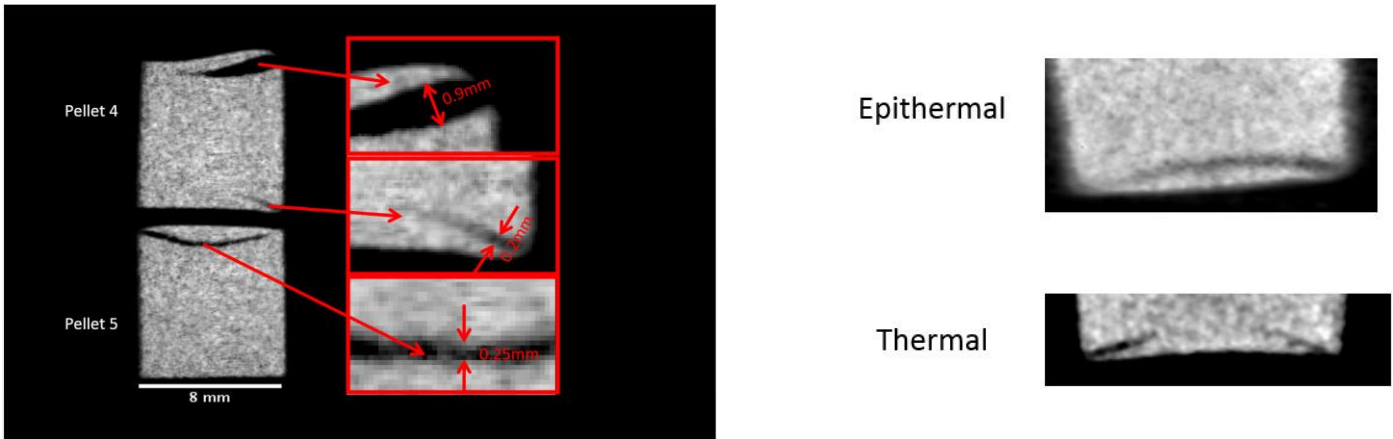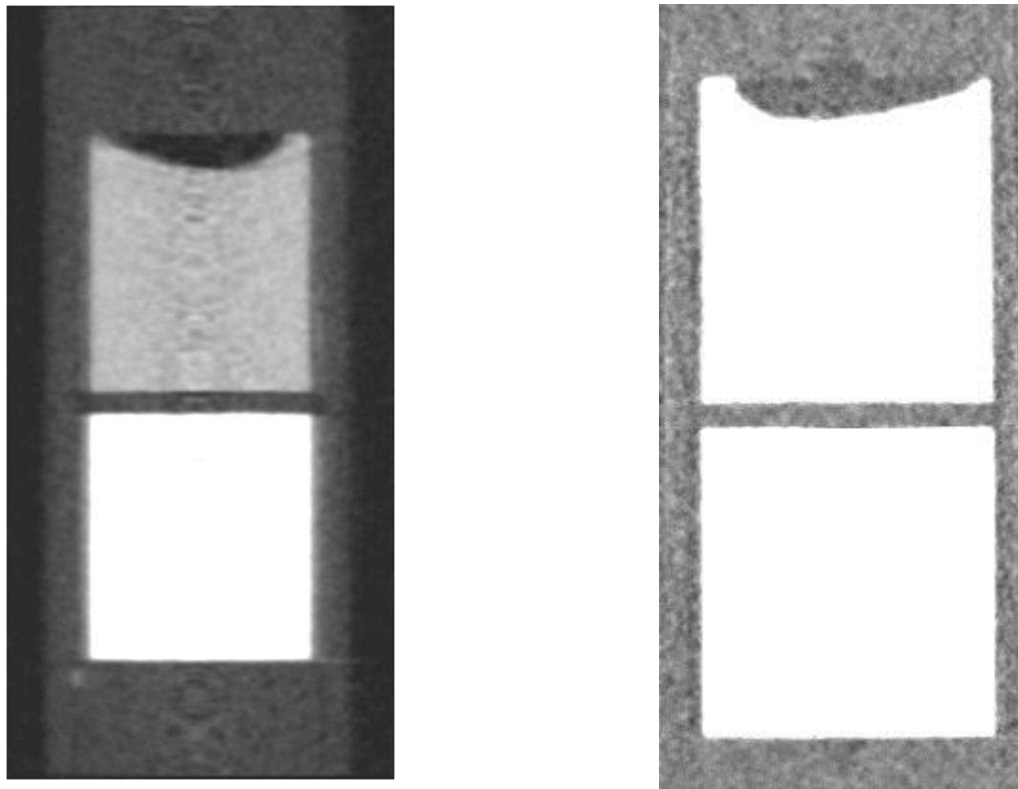specting the images and reconstructions takes experience so the data analysis reported here is preliminary. In fact a key aspect of making the techniques accessible will be facilitating the data processing and viewing and reporting of the results to identify relevant features in an efficient manner.

A significant step forward has been the quantitative determination of isotopic composition. When using Tantalum the 235-U atomic enrichment was in agreement with nominal fabrication values to within +- 0.1 atomic %. When using Cadmium the systematic underestimate of the enrichment values was ascribed to the paucity of cadmium resonances in the 1 to 50eV range and thus a poor background fit.

Potentially the shape and features of cracks can be related to stress distributions and fabrication conditions and have the potential to inform and guide synthesis parameters. The limiting spatial resolution of the detector used in these studies is 55 microns.   Improved spatial resolution is clearly desirable to approach the grain size and length scales consistent with the individual phases of the composite phases in the ATF fuels. Detector developments are underway to improve the spatial resolution and precedent at NIST and PSI suggest that 10 micron spatial resolution is possible.

The national capacity for destructive PIE of irradiated fuels is limited. The cost is large and the schedule constrained.   For these reasons there is merit in exploring the opportunity to non destructively examine irradiated fuels. At the current point in development of the neutron based techniques they have the potential to contribute mechanical integrity, phase, isotopic distribution and pellet clad interactions data for many cubic centimeters of irradiated fuel that is integral to validation of mesoscale/engineering scale models. Improved spatial resolution is a key development goal.   However the shipping cost for moving irradiated fuels between INL and LANL remains an impediment. One exciting possibility that is under consideration concerns the availability of nascent neutron production technologies using small scale accelerator and laser based sources that might be realized to enable poolside characterization at INL or industrial facilities.

8.   Future Work

    Work completed in the last 6 months not addressed here includes diffraction measurements using the HIPPO instrument on rodlets 1 and 2 and spatially resolved diffraction measurements on Rodlet 1 using the SMARTS instrument. These will be addressed in the next report with gamma ray spectroscopy activation measurements and gamma ray sensitivity measurements of the detector. Both data processing and instrument development offer opportunities to improve resolution sensitivity and measurement throughput. A meeting with representatives of the synthesis and modelling communities will discuss measurements for the next run cycle.

Instrument improvements
    Resonances measured in these studies have been measured up to 200eV. However our collaborator Anton Tremsin collected data using the same detector at the J-PARC pulsed neutron source in Japan and observed resonances up to KeV.   Thus control of the instrument background on FP-5 is a key goal to improve performance.

An MCNP model of flight path 5 indicated that some though not all of contribution to the background originates from the moderator on the opposite side of the target/moderator/reflector assembly. This moderator emits a delayed spectrum with the result that resonances that should have exhibited 0% transmission were observed with transmissions of 10-20% of the incident intensity. Unfortunately this cannot be addressed by instrument redesign.

To address other sources of background we plan to install a 5m flight tube inside the experimental cave to avoid intensity loss of ~25% due to air scatter. In addition we will replace the current steel collimation with borated steel (NEUTRONIT from Boehler, Austria). The openings at the entrance and exit will be square, to match the moderator and detector and follows the approach demonstrated at FRM-2.

In addition to the flight path collimation a separate effort will address the detector which currently employs a boron and gadolinium-doped MCP. The detector was developed for use in the thermal regime for which the Gd epithermal resonances response were irrelevant but which complicate measurements for this study. For this reason we are exploring the availability of using a boron-only MCP with higher boron concentration to improve our background measurement.

Receipt of Transuranic fuels

In the next run cycle we will examine two U-20Pu-10Zr fuel rodlets containing transuranics. Shipment and receipt of these samples to LANL by Randy Fielding is scheduled for this fiscal year. The samples are cast and scheduled for encapsulation in April 2016. Their nominal dimensions are 0.168" OD and 1.5" long. When chemical analysis and isotopic estimates are available, the Authorization basis calculations will be completed to execute transfer of the samples from INL to LANL. The possibility of repackaging archive MOX or MA-MOX pellets for examination remains of interest.

Continued assessment of potential for study of irradiated fuels

The measurements on the pre-irradiated material are valuable in their own right but a huge "payoff for this work would be to perform measurements on irradiated fuel rodlets. A key milestone test to demonstrate the viability of measurements on irradiated fuel will be a detector test to be performed by Anton Tremsin at INL in May when he will test the detector performance in the vicinity of irradiated fuel. This will demonstrate the ability of the detector to resolve the neutron measurements from the gamma induced signal from real irradiated fuels. Appendix A section 11 of this report includes a conceptual cask for handling rodlets of LANL ATF in the beam line. Discussion about handling irradiated fuel rodlets and hot cell utilization at LANL are ongoing.

9.   Conclusions

The application of non-destructive evaluation for the analysis of as-fabricated nuclear fuels has the potential to provide critical enabling data to realize science based fuels development. By characterizing fuels before irradiation it can be ensured that phenomena observed in post irradiation studies are the result of irradiation and not the initial condition of the material. Non destructive characterization of irradiated material can ensure that destructive evaluation in hot cells is used to maximum cost efficiency to study regions in samples that represent average and atypical behavior.

Neutron tomographic imaging and scattering measurements on nuclear fuels of fabrication geometries can provide non destructive measurement of cracks, flaws, chemistry, phase, texture, and fission gas pressure. The potential for data from fresh and irradiated material can contribute extensive data sets to fill gaps for modeling and simulation of irradiation effects, which have the potential to improve fuel performance codes that dictate economics and safety margins.

10. References

[1]   M.D. Roth et al. "Bright laser-driven neutron source based on the relativistic transparency of solids." Physical review letters 110, no. 4 (2013): 044802.

[2]   Brown, A., and J. J. Norreys. "Beta-Polymorphs of Uranium and Thorium Disilicides." (1959): 673-673

[3]   Dwight, A. E. Study of the uranium-aluminum-silicon system. Argonne National Lab., IL (USA), 1982.

[4]   M. B. Aufderheide III, H.-S. Park, E. P. Hartouni, P. D. Barnes, D. M. Wright, R. M. Bionta, J. D. Zumbro, C. L. Morris, "Proton radiography as a means of material characterization", AIP Conference Proceedings, **497** (1999) 706.

[5]   AS Tremsin, JB McPhate, JV Vallerga, OHW Siegmund, JS Hull, WB Feller, and E Lehmann. High-resolution neutron radiography with microchannel plates: Proof-of-principle experiments at psi. Nuclear Instruments and Methods in Physics Research Section A: Accelerators, Spectrometers, Detectors and Associated Equipment, 605(1):103–106, 2009.

[6]   Vogel et al., "Assessment of advanced NDE techniques and the path forward to evaluating an AFC-2 irradiated fuel pin", LA-UR 13-2167.

[7]   A. Tremsin, S. Vogel, M. Mocko, M. Bourke, V. Yuan, R. Nelson, D. Brown, B. Feller, "Non-destructive studies of fuel rodlets by neutron resonance absorption radiography and thermal neutron radiography", Journal of Nuclear Materials, **440** (2013) 633–646.

[8]   C. Morris, M. Bourke, D. Byler, C. Chen, G. Hogan, J. Hunter, K. Kwiatkowski, F. Mariam, K. McClellan, F. Merrill, et al., "Qualitative comparison of bremsstrahlung X-rays and 800 MeV protons for tomography of urania fuel pellets", Review of Scientific Instruments **84** (2013) 023902.

[9]   EH Lehmann, G Frei, P Vontobel, L Josic, N Kardjilov, A Hilger, W Kockelmann,and Axel Steuwer. The energy-selective option in neutron imaging. Nuclear Instruments and Methods in Physics Research Section A: Accelerators, Spectrometers, Detectors and Associated Equipment, 603(3):429–438, 2009.

[10]   Michael Schulz, Peter B¨oni, Elbio Calzada, Martin M¨uhlbauer, and Burkhard Schillinger. Energy-dependent neutron imaging with a double crystal monochromator at the antares facility at frm ii. Nuclear Instruments and Methods in Physics Research Section A: Accelerators, Spectrometers, Detectors and Associated Equipment, 605(1):33–35, 2009.

[11]   M Strobl, I Manke, N Kardjilov, A Hilger, M Dawson, and J Banhart. Advances in neutron radiography and tomography. Journal of Physics D: Applied Physics, 42(24):243001, 2009.

[12]   MB Chadwick, M Herman, P Obloˇzinsk`y, Michael E Dunn, Y Danon, AC Kahler, Donald L Smith, B Pritychenko, Goran Arbanas, R Arcilla, et al. Endf/b-vii. 1 nuclear data for science and technology: cross sections, covariances, fission product yields and decay data. Nuclear Data Sheets, 112(12):2887–2996, 2011.

[13]   http://web.ornl.gov/sci/nuclear_science_technology/nuclear_data/sammy/

[14]   Philip G Burke and Keith A Berrington. Atomic and molecular processes: an r-matrix approach. 1993.

[15]   N. LARSON, "Updated user's guide for SAMMY: multilevel R-matrix fits to neutron data using Baye's equations." No. ORNL/TM-9179. Oak Ridge National Lab., TN (USA), 1984.

[16]   M. MOCKO *et al.*, "Advantages and limitations of nuclear physics experiments at an ISIS-class spallation neutron source." Nuclear Instruments and Methods in Physics Research Section A: Accelerators, Spectrometers, Detectors and Associated Equipment 589.3 (2008): 455-464.

17　　　A. TREMSIN *et al.*, "High-resolution neutron radiography with microchannel plates: Proof-of-principle experiments at PSI." Nuclear Instruments and Methods in Physics Research Section A: Accelerators, Spectrometers, Detectors and Associated Equipment 605.1 (2009): 103-106.

11. Appendix.   Irradiated Fuel Manipulation Container

A limiting factor for applying these types of characterization to irradiated fuel, is the necessity for shielding and remote alignment capabilities for such samples at the beam line. This proposal addresses this limitation by combining a motion control suitable for neutron/proton imaging & tomography and neutron diffraction with containment designed for irradiated fuel rodlets. Our design concept is shown in Fig. 28.
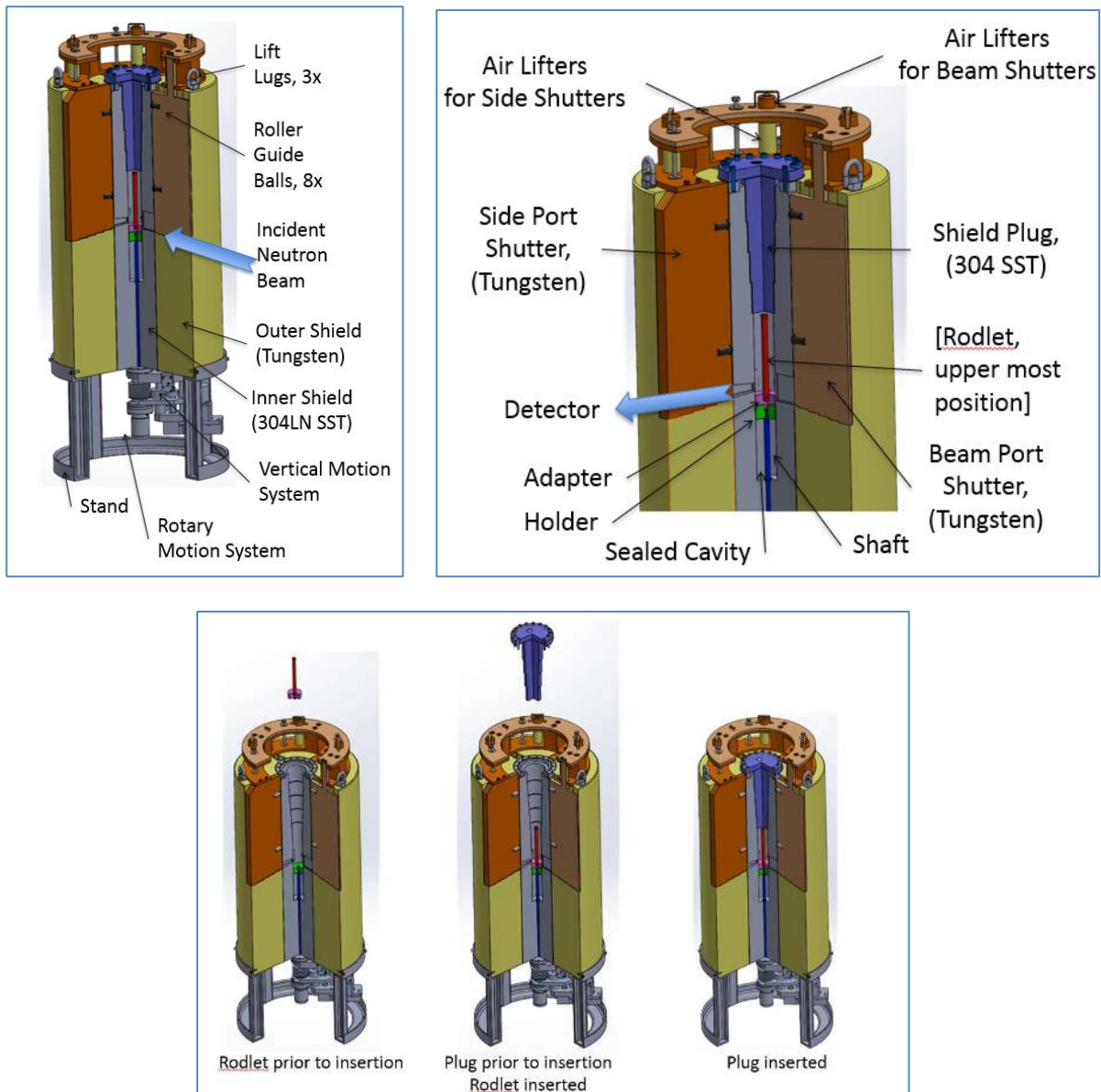

Fig. 28: Irradiated Fuel Manipulation Container for in situ examination (Design concept).

With this container any beam line at any facility capable of accommodating this assembly would be able to contribute to the characterization of irradiated materials. At LANSCE, this would include the imaging beam line on flight path 5 (for tomographic characterization and isotopic densities); the SMARTS

engineering diffractometer (e.g. for residual stress measurements or profile analysis to characterize e.g. dislocation densities), the HIPPO general purpose diffractometer (to assess phase composition and texture). Besides the neutron characterization, LANSCE offers characterization by proton radiography and tomography. With the proposed container/motion control combination, radioactive materials could be transferred between beam lines without exposing personnel to radiation, and then be characterized utilizing the shutters integrated into the container for incident, transmitted, and diffracted beams and the motion control to align, rotate, and scan them in the beam lines.

Existing shielding of experimental hutches would protect personnel when the shutters are open. The integrated rotation and translation of the sample, enabled by remote controlled motors allow one to sample rotation for tomography while probing different sections along the sample axis (e.g. for diffraction probing slices or imaging techniques with smaller field of view than the whole sample). Irradiated rodlets (or other radioactive samples) would be loaded into the container in hot cells available at LANL. The combination of all these techniques would provide unprecedented characterization of e.g. irradiated materials and thus advance the field of nuclear engineering.